Geophysical Journal International

*Geophys. J. Int.* (2011) doi: 10.1111/j.1365-246X.2011.05057.x

# The energetic 2010 $M_W$ 7.1 Solomon Islands tsunami earthquake

Andrew V. Newman,[1] Lujia Feng,[1] Hermann M. Fritz,[1,2] Zachery M. Lifton,[1] Nikos Kalligeris[3] and Yong Wei[4,5]

[1]*School of Earth and Atmospheric Sciences, Georgia Institute of Technology,* 311 *Ferst Drive, Atlanta, GA* 30332*, USA. E-mail: anewman@gatech.edu*
[2]*School of Civil and Environmental Engineering, Georgia Institute of Technology, Savannah, GA* 31407*, USA*
[3]*Department of Environmental Engineering, Technical University of Crete, Chanea, Greece*
[4]*Center for Tsunami Research, Pacific Marine Environment Laboratory, National Oceanographic and Atmospheric Administration, Seattle, WA* 98115*, USA*
[5]*Joint Institute for the Study of Atmosphere and Ocean, University of Washington, Seattle, WA* 98105*, USA*

Accepted 2011 April 26. Received 2011 April 22; in original form 2011 February 8

## SUMMARY

On 2010 January 3 a moment magnitude $M_W$ 7.1 earthquake struck the Solomon Islands very near the San Cristobal trench, causing extensive landslides and surprisingly large tsunami waves. Because of the unique proximity of islands to the trench (<20 km) and earthquake, a post-seismic survey successfully identified unexpected widespread coseismic subsidence towards the trench (up to 80 cm), with no discernable post-seismic deformation. Approximately 1000 km from the earthquake ocean-bottom pressure sensors measured 1–2 cm open-ocean tsunami waves. Though spatially limited, the local tsunami wave heights up to 7 m were comparable to the much larger adjacent 2007 $M_W$ 8.1 earthquake. The seismically determined focal mechanism, broad-scale subsidence, tsunami amplitude and open ocean wave heights are all explained by an extremely shallow low-angle thrust adjacent to the impinging subduction of the two seamounts near the trench. This event belongs to a potentially new class of shallow 'tsunami earthquakes' that is not identified as deficient in radiated seismic energy.

**Key words:** Seismic cycle; Tsunamis; Earthquake source observations; Subduction zone processes.



## INTRODUCTION

The Solomon Islands lie within one of the most active seismogenic zones globally due to the rapid and complicated convergence of the Pacific Plate with the Australian Plate and numerous microplates at approximately 10 cm yr$^{-1}$ (Miura *et al*. 2004; Phinney *et al.* 2004; Taira *et al.* 2004; Fig. 1a). This activity creates a unique environment that both: causes large and tsunamigenic earthquakes with sufficient frequency to self-sustain an oral tradition of tsunami preparedness within the indigenous populations (Fritz & Kalligeris 2008; McAdoo *et al.* 2009); and allows for detailed land-based studies of shallow subduction processes due to the development of land from permanent collisional deformation and volcanism very near the trench. In the area of the 2010 $M_W$ 7.1 earthquake, young bathymetrically elevated microplate boundaries and seamounts are subducted along the San Cristobal trench causing the development of several islands, including Rendova and Tetepare (Fig. 1b), within 10–20 km of the trench (Mann *et al.* 1998; Taylor *et al.* 2005, 2008). A complex recent history of uplift is associated with the subduction of a ridge system (270–130 ka), followed by subsidence, and recent return to very rapid uplift (∼50 ka–present) due to the initiation of Coleman and Kana Keoki Seamount subduction (Mann *et al.* 1998; Taylor *et al.* 2005). Currently, geological uplift rates are observed to rapidly increase from near zero at the northeastern end of Rendova to maximum values (5–7 mm yr$^{-1}$) on the southwestern (near-trench) edges of Rendova and Tetepare Islands (Mann *et al.* 1998; Taylor *et al.* 2005).

Past earthquakes in the Solomon Islands were highly tsunamigenic. While the 2007 $M_W$ 8.1 event is the largest instrumentally recorded local earthquake, other notable tsunamigenic earthquakes occurred over the past century. A series of earthquakes between 1925 and 1926 excited at least two tsunamis. Following a magnitude $M$ 7.2 event near Guadalcanal on 1926 April 12, a similarly sized $M$ 7.3 event on 1926 September 16 produced a tsunami that flooded western Guadalcanal and Kokomaruki islands (Soloviev & Go 1984; Engdahl & Villaseñor 2002). Both events are comparable, but estimated to be slightly larger than the 2010 event. Interestingly, with the exception of the 2007 event, the other tsunamigenic earthquakes were low-$M$ 7; normally considered too small for significant tsunami generation. While it is possible that some of these events were classic slow-source 'Tsunami Earthquakes' (TsE), such events identified to date have a very limited magnitude range (between

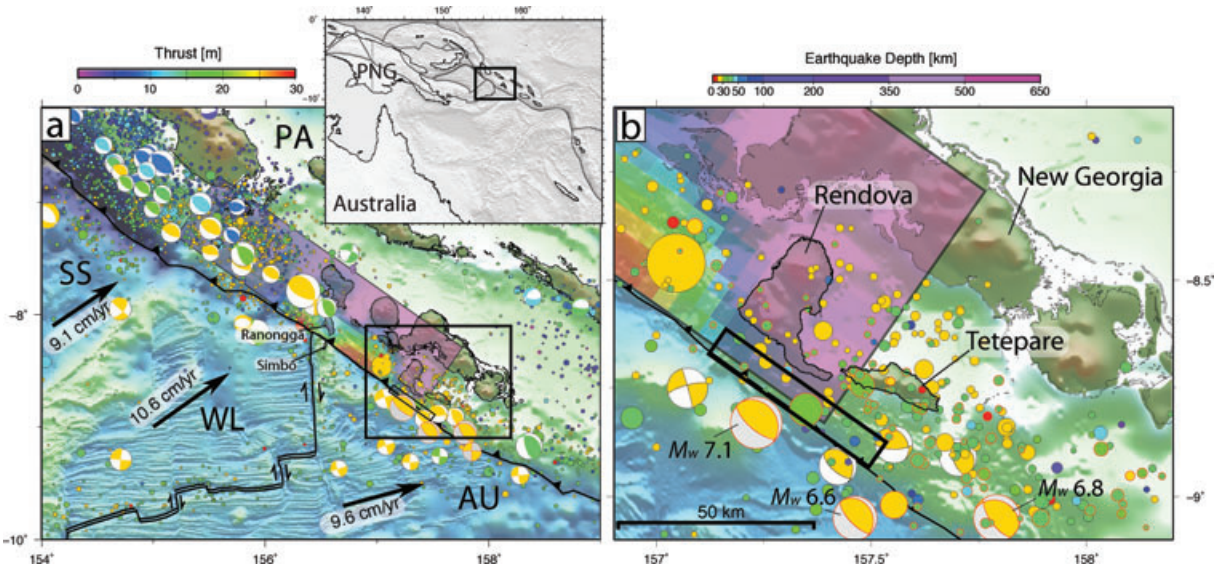


**Figure 1.** (a) Regional hypocentral earthquake locations since 1962 ($M_W \geq 4$), centroid focal mechanisms since 1976 ($M_W \geq 6$; Ekström *et al.* 2005) and regional plate boundaries and motions (Goodliffe *et al.* 1999; Bird 2003). Plate motions (arrows) are shown for the Australian (AU), Woodlark (WL) and Solomon Sea (SS) microplates relative to stable Pacific plate (PA). The modelled slip from Chen *et al*. (2009) is shown for the 2007 April 1 $M_W$ 8.1 event (diagonal rectangle). Location of (a) is shown in grey shaded-relief (box). (b) Detailed view of box in (a) illustrates the 2010 January 3 $M_W$ 7.1 event adjacent to the high slip zone of the larger 2007 earthquake. Diagonal box is the outline of the preferred megathrust model of this study. Seismicity occurring in 2010 January, including two events with $M_W \geq 6.6$ is outlined in red.

$M_W$ 7.5 and 8.1) (Kanamori 1972; Newman & Okal 1998; Ammon *et al*. 2006; Newman *et al.* 2011). Thus, while the 2010 earthquake may indeed have ruptured the near-trench environment, as suggested by gCMT depth (12 km) and location, and position relative to the observed shallow slip localization of the 2007 event (Fig. 1b), its magnitude is smaller than known slow-source TsE.

## EARTHQUAKE ENERGY AND DURATION

Other recent TsE events are well-observed to be deficient in radiated seismic energy, $E$, when compared with seismic moment, $M_0$, such that the TsE discriminant $\Theta = \mathrm{Log}_{10}(E/M_0)$ is below $-5.7$, as compared to the global thrust average, $\Theta = -4.74$ (Newman & Okal 1998; Convers & Newman 2011). Analysis of the TsE discriminant using 68 vertical broadband seismograms from global stations for the 2010 Solomon Islands earthquake define $\Theta = -4.8$, comparable to the global average for thrusting mechanism earthquakes, and unlike observed slow-source TsE (Fig. 2). Hence, if the earthquake is to be classified as a TsE, it is unique in that it is comparatively energetic in nature.

To evaluate the rupture duration $T_R$ of the 2010 event we identified the energy minimum from the envelop of stacked seismograms, aligned by the *P*-wave arrival. However, because observational duration estimates include both near-source surface reflections and can include later scattered energy after the termination of rupture, the estimated rupture duration is a maximum. Unlike the recent larger TsE events ($M_W \geq 7.7$), with rupture durations $T_R$ in excess of 100 s, the $M_W$ 7.1 2010 event has $T_R \leq 33$ s, comparable to another regional $M_W$ 7.1 earthquake in the Celebes Sea on 2009 February 11 (Fig. 2). However, given the spatial extent of the 2010 Solomon Islands event, the event may have been slow ($>$1–1.5 km s$^{-1}$ dependent on point of nucleation for a 50 km long rupture). If the event is indeed slow rupturing, it remains to explain why it does not exhibit the deficiency in radiated seismic energy observed in larger slow-source TsE.

## TSUNAMI AND SUBSIDENCE OBSERVATIONS

The 2007 $M_W$ 8.1 megathrust earthquake nucleated just west of Rendova Island and ruptured northwest for approximately 300 km (Taylor *et al.* 2008; Chen *et al.* 2009; Furlong *et al.* 2009). The earthquake created prevalent tsunami waves across the islands, with focused run-up in excess of 12 m in some locations (Fritz & Kalligeris 2008). Though tsunami waves were widespread, only 52 deaths were reported due to the rich ancestral recitation of past events, whereby the need to run to high ground immediately after shaking was understood and practiced (Fritz & Kalligeris 2008). In the 2007 event massive slip (20+ m) occurred in patches very near the trench, and within 20 km of the source region of the 2010 event near Rendova Island (Chen *et al.* 2009), suggesting the recent event was triggered (Fig. 1). The boundary between the events is concurrent with a projected break in a subducted transform fault and ridge system along the megathrust interface (Mann *et al*. 1998), likely inhibiting rupture of the 2007 event to the southeast. However, the large 20+ m slip from the 2007 event caused a stress perturbation that likely enhanced the Coulomb failure criteria (Stein 1999), and positively influenced the occurrence of the adjacent 2010 earthquake, similar to the stress induced by the $M_W$ 9.1 2004 Sumatra–Andaman earthquake, on the $M_W$ 8.7 2005 earthquake in Sumatra; forecasted by McCloskey *et al.* (2005).

Though far smaller than the expected magnitude for significant regional tsunami excitation, the $M_W$ 7.1 2010 event created a local tsunami run-up that was only moderately smaller than the much larger $M_W$ 8.1 2007 event (Fig. 3). Based on initial reports of villages inundated by tsunami waves and identification of tsunami

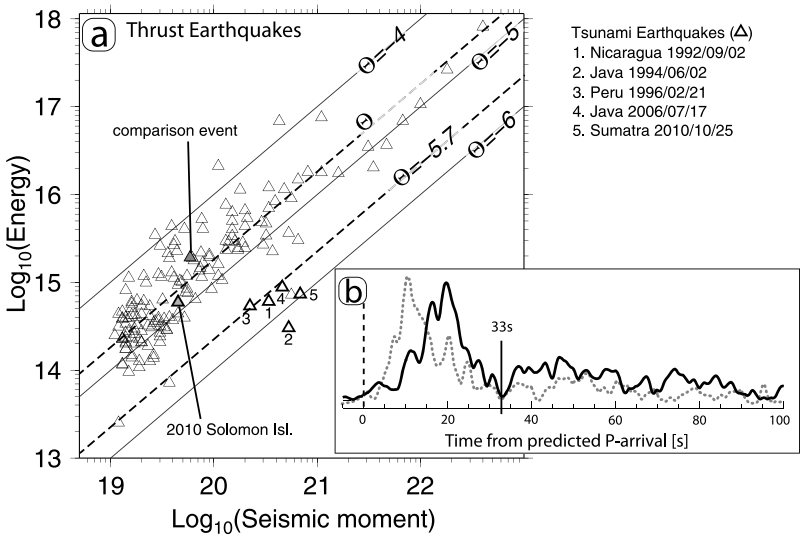


**Figure 2.** (a) Shown is a comparison of energy-to-moment ratios for global thrust earthquakes between 1997 and mid-2010, including known tsunami earthquakes since 1992 and the 2010 Solomon Islands earthquake (Newman & Okal 1998; Convers & Newman 2011; Newman *et al.* 2011). Unlike other known tsunami earthquakes that consistently report very low radiated seismic energy, the 2010 Solomon Islands earthquake generated normal radiated seismic energy ($\Theta = -4.8 \pm 0.3$, using 68 stations $25^\circ \leq \Delta \leq 80^\circ$). (b) The envelope of the stacked vertical broadband seismograms reveals an estimate of the rupture duration (33 s) for the 2010 Solomon Islands earthquake, significantly shorter than the 5 observed slow-source tsunami earthquakes (duration >100 s), and similar to another recent regional $M_W$ 7.1 event used for comparison; a shallow (depth = 23 km) megathrust event in the Celebes Sea on 2009 February 11 [grey dashed line in (b) and grey triangle in (a)]. The stacked envelopes show that while the more energetic comparison event peaks earlier its duration is similar.

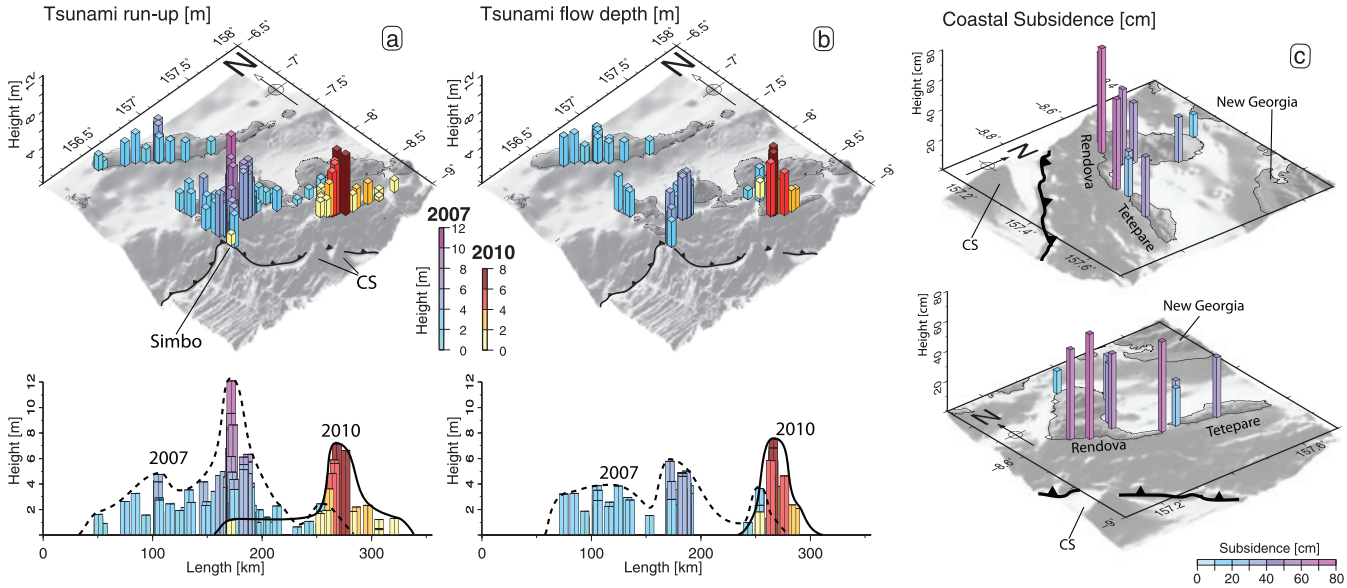


**Figure 3.** Tsunami (a) run-ups and (b) flow depths are shown for both the 2007 $M_W$ 8.1 (cool colours) from Fritz & Kalligeris (2008) and the 2010 $M_W$ 7.1 (hot colours) Solomon Islands earthquakes. Maximal tsunami impact in the 2010 earthquake is near the now subducting double-peaked Coleman Seamount (CS) structures. Flow depths, though harder to measure, yield a more precise estimate of tsunami height. The order of magnitude smaller 2010 earthquake caused larger localized flow depths, and only moderately smaller run-ups. No significant tsunami impact occurred in the western 30 per cent of the 2007 earthquake zone (area not shown). (c) Two views of land-level change observed across Tetepare and Rendova Islands from the $M_W$ 7.1 earthquake. Though uplift was expected from megathrust rupture, only subsidence was found, with a maximum (–80 cm) in the near-trench region. Data were collected over a 5-d period beginning 9 d after the main shock, and consisted primarily of submerged natural and anthropogenic markers. White diamonds represent four points where land-level changes were not discernible.

waves on two ocean-bottom pressure sensors termed DART buoys (or Deep-Ocean Assessment and Reporting of Tsunamis) nearly 1000 km away (NOAA 2010), we investigated the extent of tsunami inundation and coseismic and early post-seismic deformation. Between January 12 and 19 we surveyed tsunami inundation, run-up, and coastal land-level changes, and established a rapid post-seismic deployment of five Global Positioning System (GPS) stations in the area. Tsunami and land level surveys were made at 21 sites surrounding Rendova, Tetepare, South (Marovo Lagoon) and Simbo Islands (Figs 1 and 3). No tsunami measurements were made on

Ranongga Island, however local individuals described some small waves similar to a 'fast tide', but since the island was uplifted by 3 m in 2007, villages are now far from beaches and tsunami effects are difficult to observe. The opposite is true for Simbo Island, which subsided 2 m in the 2007 event and recorded 1.2 m tsunami run-up in 2010. GPS measurements were focused on four stations in the near-source region of Tetepare and Rendova Islands for determination of early post-seismic deformation relative to a base station established on Lola Island (Fig. S1).

The survey team documented tsunami land-level changes as well as tsunami run-up, flow depth and inundation; identifying wave induced deposition or erosion, structural damage and interviewed eyewitnesses following established protocols (Synolakis & Bernard 2006). The tsunami arrived at mean sea levels during a rising tide, and all survey measurements were corrected for tide based on predictions (UHKO 2010). Significant variations in tsunami impact was observed across Rendova and Tetepare Islands, with a maximum flow depth (7.5 m) and run-up (7 m) on the southern shores of Rendova (Fig. 3). Fortunately only two villages, Mbaniata and Retavo (299 and 10 inhabitants, respectively), were significantly inundated (up to 150 m from the coast), and only two minor injuries occurred while villagers were evacuating because of strong ground shaking. In Mbaniata 16 houses (compared to only four in 2007) and the entire village of Retavo were destroyed (Fig. S2). Tsunami wave heights from the 2010 event exceeded those from 2007 across most of the two islands. Further away, tsunami run-up over 1 m was documented at South Island (50 km east) and at Simbo Island (90 km west). Smaller tsunami waves (<1 m) were observed throughout the New Georgia group including the south shores of Ranongga and Ghizo Islands.

Throughout the affected area, eyewitnesses reported one to five main waves usually with an initial recession, which could correspond to a leading depression N-wave (Tadepalli & Synolakis 1994). At most locations, the first wave arrived within 10 min of the earthquake. A second smaller wave shortly followed within another 10 min along the south coast of Rendova (see Supporting Information for further tsunami survey details).

Coastal subsidence was measured at boat launches, and navigation and port infrastructure using pre- and post-event high tide water lines and eyewitness accounts. At several locations subsidence measurements where made both in 2007 (Fritz & Kalligeris 2008), and 2010 along identical transects based on GPS waypoints and photographic documentation. At some locations such as Rendova Harbour identical eyewitnesses were interviewed in 2007 and 2010.

Though substantial afterslip was observed in the shallow megathrust following large earthquakes including the 2005 Sumatra (Hsu *et al.* 2006), and likely the 2007 Solomon Islands earthquakes (Chen *et al.* 2009), GPS observations here revealed no discernible afterslip at our survey locations (Fig. S3). However, the observation of no uplift and widespread sub-metre subsidence with maximum values nearest the trench are intriguing (Fig. 3c), as they are opposite in sense from both the expected hanging wall motion of a megathrust rupture, and the rapid short-term geological uplift across the islands (Mann *et al.* 1998; Taylor *et al.* 2005).

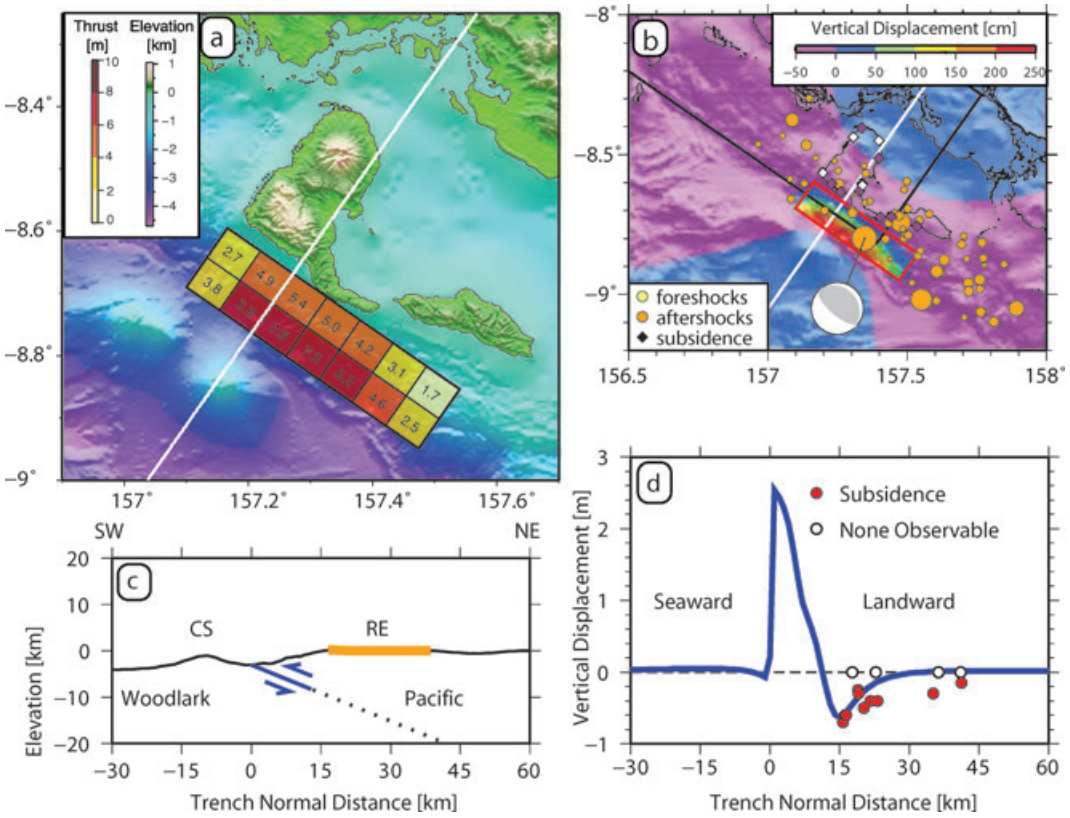


**Figure 4.** (a) The optimal distributed shallow megathrust slip model is shown for the (b) measured subsidence (diamonds) and predicted vertical deformation (red box highlights model in (a)). (c) Subduction zone profile along the white line in (a) shows the downdip extent of the TsE model predicted by the gCMT mechanism. Rendova Island (RE) is shown in orange. (d) Projected subsidence measurements (circles) along the modelled vertical deformation (blue line) are shown for the profile in (b). A high angle intraslab event also fits observed subsidence data but not the observed tsunami (Figs S3 and S7).

## DEFORMATION MODELLING

The gCMT focal mechanism for this event suggests shallow thrusting along the plate interface downdip of the San Cristobal trench (Ekström *et al.* 2005). However, a shortcoming of far-field seismic techniques, as is used for gCMT determinations, is the inability to distinguish between the true fault and auxiliary planes. With near-field deformation measurements such an ambiguity may be resolved. Thus, we tested models with the observed regional subsidence for both low-angle slip (dip = 22°) along the megathrust and high-angle slip along an orthogonal intraslab plane. For slip along the megathrust, in order to explain the observed increasing subsidence of sites nearer the trench it is necessary to allow slip only along a narrow strip between the southern shore of the nearby islands and the trench (downdip width = 13 km). This is because substantial slip further downdip would require uplift rather than subsidence of the trenchward component of Rendova and Tetepare islands.

We inverted for variable thrust along the shallow megathrust using smoothed Okada (1992) dislocation model, similar to that described in Chen *et al.* (2009) for the 2007 event. Our optimal rupture model requires 6+ m of thrust along a 30 km segment in the upper half of the modelled fault. Assuming average crustal rigidity (30 GPa), the extent and magnitude of slip corresponds to

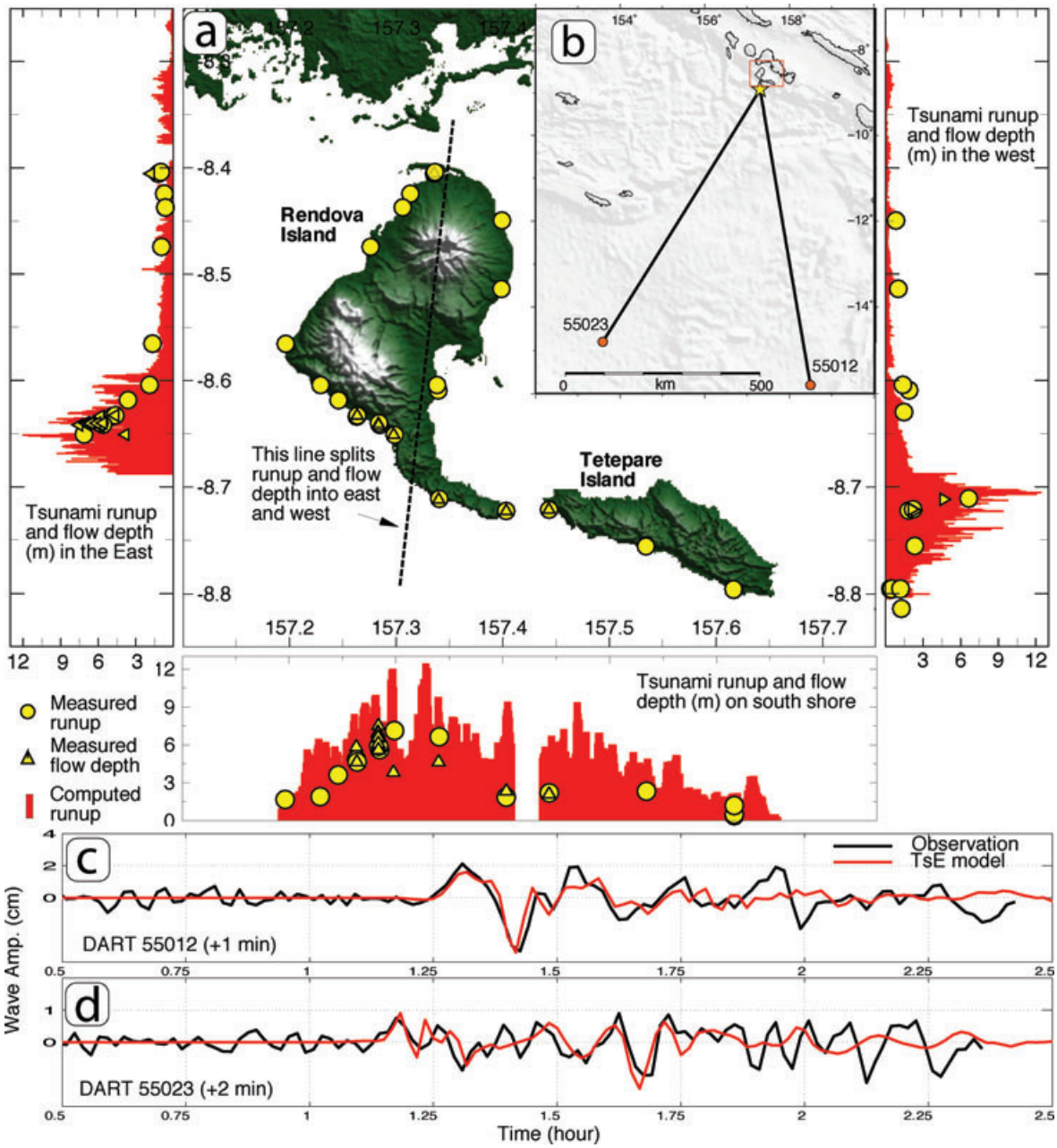


**Figure 5.** Comparison of observed tsunami data and model predictions using seafloor displacements estimated from the earthquake slip model in Fig. 4. (a) The spatial distribution of predicted (red bars) and observed tsunami run up and flow depths (yellow circles and triangles) are projected along the south shore, and along the eastern and western sides of the islands (separated by dashed black line). (b) Two ocean-bottom pressure sensors approximately 1000 km south of the event (c and d) measured cm level open-ocean tsunami heights, which are well predicted by the tsunami model.

an $M_W$ 7.2 earthquake that yields the proper direction, shape and magnitude of motion, with rms misfit (0.18 m) comparable to error in subsidence measurements (Fig. 4; see Supporting Information for details). The slight increase in magnitude over the seismically resolved $M_W$ 7.1 may be due to either early afterslip occurring in the week prior to our arrival, or an un-modelled reduction in the local shallow rigidity allowing increased slip for the same seismically observed moment release (Bilek & Lay 1999).

An alternative high-angle thrust model requires larger slips, but with comparable RMS misfit (0.18 m). Given the teleseismic mechanism and the locations of the one-sided geodetic observations, the high-angle intraslab result is not distinguishable from the shallow megathrust model.

## TSUNAMI MODELLING

To distinguish between these two models we compare the predicted tsunami run up and open-ocean tsunami wave height time series as recorded by DART sensors. Because tsunami excitation from earthquakes is predominantly controlled by the amplitude and spatial extent of vertical seafloor deformation, the high-angle intraslab and low-angle megathrust models can be differentiated due to the larger amplitude and shorter wavelength deformation produced by the high-angle thrust model.

Using the vertical predicted seafloor deformation from the two distributed slip models, we estimated the tsunami wave time series at the DART stations as well as coastal runup around Tetepare and Rendova Islands using the MOST tsunami model (Titov & Synolakis 1998). MOST computes tsunami propagation and inundation using multiscale grids of increased resolution nearest the coast (in this case moving from 36 inches in open ocean to 3 inches nearest the shore). The shallow thrusting TsE model produced surprisingly accurate predictions of the observed run up and open-ocean DART wave heights (Fig. 5), while the high-angle model consistently over-predicted tsunami heights by a factor of 2 or more (Fig. S7). Modest local differences in run up can occur due to inaccuracies in the near-shore bathymetry. Of particular note, the DART wave heights accurately predict the first wave-heights in both amplitudes and frequencies. Shifts of 1–2 min in the model are necessary to match the timing, and can be attributed to finite source duration (∼30 s; see Fig. 2) that is not considered in the tsunami model, and small inaccuracies in the absolute open-ocean bathymetry (1–2 per cent). Though splay faults have been observed in the shallow trench, and proposed to cause increased tsunami excitation in TsE (Moore *et al.* 2007), such a high-angle vertical fault was unnecessary to explain the observed tsunami field.

The very large tsunami run up commensurate with an earthquake an order of magnitude larger clearly identifies this event as a tsunami earthquake given its original definition (Kanamori 1972). Like other TsE events, the earthquake occurred in the shallowest trench environment (Polet & Kanamori 2000; Ammon *et al.* 2006; Newman *et al.* 2011). However because the radiated seismic energy is comparable to other earthquakes of its size, its was not identified as a TsE using the current $E/M_0$ discriminant (Newman & Okal 1998). It is unclear why the earthquake energetically ruptured the shallow TsE region. However, the likely recent subduction of an active ridge (Mann *et al.* 1998), and the onset of subduction of the geologically young Coleman and Kana Keoki seamounts likely contribute to increased stress and thermally controlled frictional behaviour (Figs 3 and S8). Given the history of frequent tsunamis from low $M$ 7 events in the early 20th century, it is possible that TsE's are a common feature in this region, however a lack of digital broad-band seismic data would make the energy determinations of earlier events difficult or impossible.

## CONCLUSION

Utilizing the near-trench deformation, tsunami run up and open-ocean wave height data, we identified the 2010 January 3 Solomon Islands earthquake as a shallow low-angle earthquake occurring along the megathrust along the front of the impinging seamounts. Due to the recent development of seafloor pressure sensors, and the unique occurrence of land (and hence geodetic observation) very near the trench, we were able to constrain the broad-scale coseismic subsidence and the shape of the observed open-ocean tsunami wave field. These data were instrumental in identifying the extensive shallow thrusting TsE. Without such data, the event would have likely been attributed to undocumented underwater landslides. This event belongs to a previously undocumented class of shallow energetic tsunami earthquakes.

## ACKNOWLEDGMENTS

We thank S. Weinstien, A. Lomax and an anonymous reviewer for careful reviews of the manuscript. Comments from Lomax and the anonymous reviewer helped guide us to reconsider the low-angle thrust model. NSF EAR-1020239, SAR data and GPS equipment were provided by the UNAVCO with support from NSF and NASA under EAR-0735156.

## REFERENCES

Ammon, C.J., Kanamori, H., Lay, T. & Velasco, A.V., 2006. The 17 July 2006 Java tsunami earthquake, *Geophys. Res. Lett.,* **33,** L24308, doi:10.1029/2006GL028005.

Bilek, S.L. & Lay, T., 1999. Rigidity variations with depth along interplate megathrust faults in subduction zones, *Nature,* **400,** 443–446.

Bird, P., 2003. An updated digital model of plate boundaries, *Geochem. Geophys. Geosyst.,* **4,** doi: 10.1029/2001GC000252.

Chen, T., Newman, A.V., Feng, L. & Fritz, H.M., 2009. Slip distribution from the 1 April 2007 Solomon Islands Earthquake: a unique image of near-trench rupture, *Geophys. Res. Lett.,* **36,** L16307, doi: 10.1029/2009GL039496.

Convers, J.A. & Newman, A.V., 2011. Global evaluation of earthquake energy to moment ratio from 1997 through mid-2010: with improvement for real-time energy estimation, *J. geophys. Res, in press*.

Ekström, G., Dziewonski, A.M., Maternovskaya, N.N. & Nettles, M., 2005. Global seismicity of 2003: centroid-moment-tensor solutions for 1087 earthquakes. *Phys. Earth planet. Inter.,* **148,** 327–351.

Engdahl, E.R. & Villaseñor, A., 2002. Global seismicity: 1900–1999, *International Handbook of Earthquake and Engineering Seismology*, pp. 665–690, ed. Lee, W.H.K., Academic Press, Amsterdam.

Fritz, H.M. & Kalligeris, N., 2008. Ancestral heritage saves tribes during 1 April 2007 Solomon Islands tsunami, *Geophys. Res. Lett.,* **35,** L01607, doi: 10.1029/2007GL031654.

Furlong, K., Lay, T. & Ammon, C.A., 2009. Great earthquake rupture across a rapidly evolving three-plate boundary, *Science,* **324,** 226–229.

Goodliffe, A., Taylor, B. & Martinez, F., 1999. Data report: Marine geophysical surveys of the Woodlark Basin region, *Proc. ODP, Init. Repts*., Vol. 180, pp. 1–20, eds Taylor, B. et al., Texas A&M University College Station, TX (CD-ROM).

Herring, T.A., King, R.W. & McClusky, S.C., 2008. *Introduction to GAMIT/GLOBK*, Release 10.3, MIT, Cambridge, MA.

Hsu, Y.J. *et al*., 2006. Frictional afterslip following the 2005 Nias-Simeulue earthquake, Sumatra. *Science* **312,** 1921–1926.

Jónsson, S., Zebker, H., Segall, P. & Amelung, F., 2002. Fault slip distribution of the 1999 $M_W$ 7.1 Hector Mine earthquake, California, estimated from satellite radar and GPS measurements, *Bull. seism. Soc. Am.,* **92,** 1377–1389.

Kanamori, H., 1972. Mechanism of Tsunami earthquakes., *Phys. Earth planet. Int.,* **6,** 346–359.

Mann, P., Taylor, F.W., Lagoe, M.B., Quarles, A. & Burr, G., 1998. Accelerating late Quaternary uplift of the New Georgia Island group (Solomon Island arc) in response to subduction of the recently active Woodlark spreading center and Coleman seamount., *Tectonophysics,* **295,** 259–306.

McAdoo, B.G., Moore, A. & Baumwoll, J., 2009. Indigenous knowledge and the near field population response during the 2007 Solomon Islands tsunami, *Nat. Hazards,* **48,** 73–82.

McCloskey, J., Nalbant, S.S. & Steacy, S., 2005. Earthquake risk from co-seismic stress, *Nature,* **434,** 291.

Miura, S., Suyehiro, K., Shinohara, M., Takahashi, N., Araki, E. & Taira, A., 2004. Seismological structure and implications of collision between the Ontong Java Plateau and Solomon Island Arc from ocean bottom seismometer—airgun data, *Tectonophysics,* **389,** 191–220.

Moore, G.F, Bangs, N.L., Taira, A., Kuramoto, S., Pangborn, E. & Tobin, H.J., 2007. Three-dimensional splay fault geometry and implications for tsunami generation, *Science,* **318**(5853), 1128–1131, doi:10.1126/science.1147195.

NOAA, 2010. Tsunami event—January 3, 2010 Solomon Islands, available at: http://nctr.pmel.noaa.gov/solomon20100103/ (last accessed 2011 February 8).

Newman, A.V. & Okal, E.A., 1998. Teleseismic estimates of radiated seismic energy: the *E/M*0 discriminant for tsunami earthquakes, *J. geophys. Res.,* **103,** 26 885–26 898.

Newman, A.V., Hayes, G., Wei, Y. & Convers, J.A., 2011. The 25 October 2010 Mentawai Tsunami earthquake, from real-time discriminants, finite-fault rupture, and tsunami excitation, *Geophys. Res. Lett.,* **38,** L05302, doi:10.1029/2010GL046498.

Okada, Y., 1992. Internal deformation due to shear and tensile faults in a half-space, *Bull. seism. Soc. Am.,* **82,** 1018–1040.

Phinney, E.J., Mann, P., Coffin, M.F. & Shipley, T.H., 2004. Sequence stratigraphy, structural style, and age of deformation of the Malaita accretionary prism (Solomon arc–Ontong Java Plateau convergent zone), *Tectonophysics,* **389,** 221–246.

Polet, J. & Kanamori, H., 2000. Shallow subduction zone earthquakes and their tsunamigenic potential, *Geophys. J. Int.,* **142**(3), 684–702.

Soloviev S.L. & Go Ch. N., 1984. *A Catalogue of Tsunamis on the Western Shore of the Pacific Ocean,* Nauka Publishing House, Moscow, 308 p. [English translation: Soloviev S.L., Go Ch.N].

Stein, R., 1999. The role of stress transfer in earthquake occurrence, *Nature,* **402,** 605–609.

Sylonakis, C.E. & Bernard, E.N., 2006. Tsunami science before and beyond Boxing Day 2004, *Phil. Trans. R. Soc.,* **364,** 2231–2265.

Tadepalli, S. & Synolakis, C.E., 1994. The run-up of N-waves on sloping beaches, *Proc. R. Soc. A,* **445,** 99–112.

Taira, A., Mann, P. & Rahardiawan R., 2004. Incipient subduction of the Ontong Java Plateau along the North Solomon trench, *Tectonophysics,* **389,** 247–266.

Taylor, F.W., *et al*., 2005. Rapid forearc uplift and subsidence caused by impinging bathymetric features: examples from the New Hebrides and Solomon arcs, *Tectonics,* **24,** doi: 10.1029/2004TC001650.

Taylor, F.W., Briggs, R.W., Frohlich, C., Brown, A., Hornbach, M., Papabatu, A.K., Meltzner, A.J. & Billy, D., 2008.Rupture across arc segment and plate boundaries in the 1 April 2007 Solomons earthquake, *Nat. Geosci.,* **1,** 253–257.

Titov, V.V., & Synolakis, C.E., 1998. Numerical modeling of tidal wave runup, *J. Waterw. Port Coastal Ocean Eng.,* **124**(4), 157–171.

UKHO, 2010. Admiralty EasyTide, available at: http://easytide.ukho.gov.uk (last accessed 2011 February 8).

## SUPPORTING INFORMATION

Additional Supporting Information may be found in the online version of this article:

**Figure S1.** 15-s kinematic GAMIT-TRACK (Herring *et al*. 2008) solutions (plotted as 5-min averages) of the post-seismic GPS survey relative to base-station ZIPO show no discernable deformation in the near-trench environment.

**Figure S2.** Tsunami impact on Rendova Island.

**Figure S3.** (a, b) Predicted vertical surface deformation and (c, d) modeled slip differences are shown for the 2010 January 3 $M_W$ 7.1 Solomon Islands earthquake between the best-estimate megathrust tsunami earthquake (TsE) and intraslab event, respectively (similar to Fig. 3).

**Figure S4.** (a, b) Tests for optimal locking depth (base of slip) for the shallow megathrust tsunami earthquake (TsE) and high-angle models.

**Figure S5.** (a–d) Model results are shown for a range of smoothing parameters. Because independent determination of individual patches in the $7 \times 2$ grid slip model is impossible given the scarcity and location of data, smoothing is applied (Jónsson *et al*. 2002; Chen *et al*. 2009).

**Figure S6.** Checkerboard test identifying the resolvability of individual patches of slip given an alternating (a) input model of 0's and 1's.

**Figure S7.** Alternative predicted (a) tsunami inundation (green bars) and open-ocean (c) tsunami wave heights at (c) dart buoys 1000 km to the south (locations shown in b) compared to the preferred model (red bars, repeated from Fig. 5), but includes both TsE (red) and high-angle fault (green) model predictions for open-ocean tsunami waves without a time-correction.

**Figure S8.** Perspective view of the earthquake source region and predicted tsunami wave heights 10 min after rupture (maximum amplitudes 1.4 m).

Please note: Wiley-Blackwell are not responsible for the content or functionality of any supporting materials supplied by the authors. Any queries (other than missing material) should be directed to the corresponding author for the article.